Supporting Information

Guest-induced proton conductivity of two-dimensional layered hydrogen-bonded organic frameworks

Jianjian Yang,[a] Jianbo Yin,[b] Qinglei Guo,[a] Changsong Xie,[a] Qianqian Yang,[b] Zhihui Kong,[a] Zixi, Kang,[a] Rongming Wang,[a,*] Daofeng Sun[a]

[a] State Key Laboratory of Heavy Oil Processing, School of Materials Science and Engineering, China University of Petroleum (East China), Qingdao Shandong 266580,
[b] People's Republic of China;. E-mail: rmwang@upc.edu.cn;
College of Science, China University of Petroleum (East China), Qingdao Shandong 266580, China.

Table S1. Crystallographic data of BPPA-azo, BPPA-gua and BPPA[1].

	BPPA-azo	BPPA-gua	BPPA
empirical formula	$C_{14}H_{15}N_3O_6P_2$	$C_{13}H_{17}N_3O_6P_2$	$C_{12}H_{12}O_6P_2$
formula weight	383.28	373.24	314.16
temperature (K)	293	293	293
crystal system	triclinic	monoclinic	monoclinic
space group	*P-1*	$P2_1/c$	$P2_1/c$
a (Å)	9.5241(3)	16.0962(3)	13.0552(18)
b (Å)	10.4051(6)	14.3676(3)	7.0852(10)
c (Å)	17.8775(8)	6.77280(10)	6.7287(13)
α (deg)	77.976(4)	90	90
β (deg)	78.130(3)	97.203(2)	98.176(14)
γ (deg)	72.036(4)	90	90
volume (Å^3)	1629.15(14)	1553.94(5)	616.07(17)
Z	2	2	2
ρcalc (g/cm^3)	1.562	1.595	1.694
μ (mm^{-1})	2.792	2.905	0.377
F (000)	792.0	781.0	324.0
Data/params	6113/491	2923/253	1246/109
GOF on F^2	1.041	1.077	0.976
final *R*	$R_1 = 0.0366$	$R_1 = 0.0379$	$R_1 = 0.0358$
indices [$I > 2\sigma(I)$]	$wR_2 = 0.1010$	$wR_2 = 0.0941$	$wR_2 = 0.0789$

Table S2. The lengths (Å) and angles (°) of hydrogen bonds of BPPA.

Donor-H···Acceptor	D-H	H···A	D···A	D-H···A
O (1)-H (1) ··O (2)	0.83	1.72	2.546	170
O (3)- H (2) ··O (2)	0.83	1.74	2.568	170

Table S3. The lengths (Å) and angles (°) of hydrogen bonds of BPPA-azo (* denotes charge assisted hydrogen bonds between cationic species and phospholates).

Donor- H···Acceptor	D-H	H···A	D···A	D-H···A
*N(1)-H(1A) ···O(3)	0.94	1.76	2.681	165
O(2)-H(2A) ···O(12)	0.94	1.64	2.566	169
N(2)-H (2B) ··O(7)	0.94	1.74	2.639	160
*N(4)-H (4A) ··O(9)	0.94	1.78	2.706	169
O(5)-H (5) ··O(3)	0.95	1.52	2.472	175
N(5)-H (5B) ··O(4)	0.93	1.78	2.690	165
O(6)-H (6) ··O(7)	0.94	1.62	2.550	168
O(8)-H (8) ··O (4)	0.94	1.65	2.591	173
O(10)-H(10) ··O(1)	0.94	1.56	2.483	170
O(11)-H(11) ··O(9)	0.94	1.62	2.554	176

Table S4. The lengths (Å) and angles (°) of hydrogen bonds of BPPA-gua (* denotes charge assisted hydrogen bonds between cationic species and phospholates).

Donor-H···Acceptor	D-H	H···A	D···A	D-H···A
*N(1)-H(1A) ··O(1)	0.91	2.16	2.979	150
N(1)-H(1B) ··O(4)	0.92	2.06	2.968	171
*N(2)-H(2A) ··O(2)	0.91	2.00	2.910	173
N(2)-H(2B) ··O(5)	0.91	2.05	2.936	163
O(3)-H(3) ··O(1)	0.86	1.71	2.569	177
*N(3)-H(3B) ··O(2)	0.91	2.33	2.978	128
*N(3)-H(3C) ··O(1)	0.91	2.15	2.967	148
O(5)-H(5) ··O(2)	0.86	1.59	2.453	175
O(6)-H(6) ··O(4)	0.86	1.63	2.494	173

Table S5. Humidity-dependent proton conductivity (S cm^{-1}) of three HOFs.

Conditions	BPPA-azo	BPPA-gua	BPPA
80°C, 60%RH	6.88×10^{-8}	4.31×10^{-8}	1.35×10^{-3}
80°C, 70%RH	2.87×10^{-7}	2.21×10^{-7}	2.34×10^{-3}
80°C, 80%RH	5.63×10^{-7}	5.32×10^{-7}	5.50×10^{-3}
80°C, 90%RH	1.85×10^{-6}	9.43×10^{-7}	2.35×10^{-2}
80°C, 95%RH	9.43×10^{-6}	3.21×10^{-6}	5.14×10^{-2}

Table S6. Temperature-dependent proton conductivity (S cm^{-1}) of three HOFs.

Conditions	BPPA-azo	BPPA-gua	BPPA
40°C, 95%RH	2.01×10^{-6}	4.06×10^{-7}	2.83×10^{-2}
50°C, 95%RH	3.09×10^{-6}	5.02×10^{-7}	3.33×10^{-2}
60°C, 95%RH	4.27×10^{-6}	5.99×10^{-7}	3.90×10^{-2}
70°C, 95%RH	6.38×10^{-6}	7.66×10^{-7}	4.72×10^{-2}
80°C, 95%RH	9.59×10^{-6}	3.05×10^{-6}	5.02×10^{-2}

Table S7. Parameters of equivalent circuit model for HOFs (80 °C, 95% RH).

	R1 (Ω)	C1 (F)	R2 (Ω)	W-R (Ω)	W-T	W-P
BPPA	52	0.05	125	48	18	0.23
BPPA-azo	119	0.21	724580	1023	43	0.61
BPPA-gua	98	0.18	638690	4524	88	0.32

Table S8. The proton conductivities (S cm^{-1}) of reported HOF materials.

	Compound Name	Conductivity	Conditions	References
1	FCF-1[2]	1.2×10^{-1}	100 °C, 98% RH	*ACS Appl. Mater. Interfaces 2019*
2	UPC-H3[3]	9.0×10^{-2}	80 °C, 99% RH	*Cryst. Growth Des. 2020*
3	HOF-H4TCPB[4]	5.9×10^{-2}	90 °C, 100% RH	*J. Membr. Sci. 2022*
4	BPPA	5.1×10^{-2}	80 °C, 95% RH	*This work*
5	BIP[5]	3.2×10^{-2}	95 °C, 95% RH	*J. Am. Chem. Soc. 2019*
6	HOF-GS-11[6]	1.8×10^{-2}	30 °C, 95% RH	*Angew. Chem. Int. Ed. 2016*
7	HOF-GS-10[6]	7.5×10^{-3}	85 °C, 90% RH	*Angew. Chem. Int. Ed. 2016*
8	CPOS-2[7]	3.7×10^{-3}	100 °C, 98% RH	*Angew. Chem. Int. Ed. 2018*
9	CB[6]·1.2H_2SO_4·6.4H_2O[8]	1.3×10^{-3}	25 °C, 98% RH	*Angew. Chem. Int. Ed. 2011*
10	$(H_{12}RCC1)^{12+}$12Cl^-·4H_2O[9]	1.1×10^{-3}	30 °C, 95% RH	*Nat. Commun. 2016*
11	CPOS-1[7]	6.0×10^{-4}	30 °C, 98% RH	*Angew. Chem. Int. Ed. 2018*
12	HOF 1[10]	4.8×10^{-4}	100 °C, 98% RH	*New J. Chem. 2023*
13	MA-B-BDC[11]	4.3×10^{-4}	50 °C, 98% RH	*Cryst. Growth Des. 2021*
14	CPOS-3[7]	3.7×10^{-4}	30 °C, 98% RH	*Angew. Chem. Int. Ed. 2018*
15	MA-TMA[11]	3.1×10^{-4}	70 °C, 98% RH	*Cryst. Growth Des. 2021*
16	HOF-H_3L[12]	6.9×10^{-5}	30 °C, 98% RH	*New J. Chem. 2019*
17	CPOS-4[7]	5.6×10^{-5}	30 °C, 98% RH	*Angew. Chem. Int. Ed. 2018*
18	BPPA-azo	9.6×10^{-6}	80 °C, 95% RH	*This work*
19	HOF 6[13]	3.4×10^{-6}	27 °C, 97% RH	*Cryst. Growth Des. 2016*
20	BPPA-gua	3.2×10^{-6}	80 °C, 95% RH	*This work*

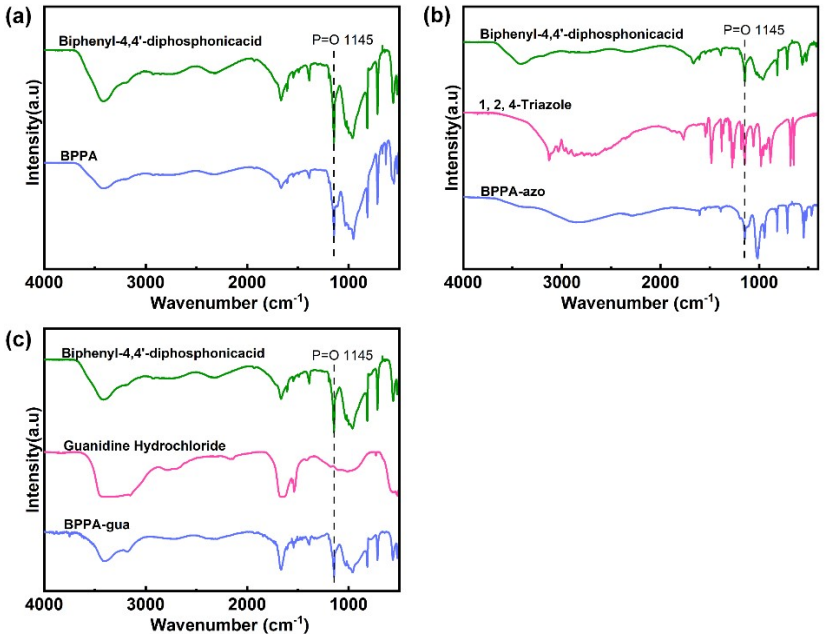

Figure S1. FT-IR spectra of biphenyl-4,4-bisphosphonic acid, 1,2,4-triazole and BPPA (a), biphenyl-4,4-bisphosphonic acid, guanidine hydrochloride and BPPA-azo (b); biphenyl-4,4-bisphosphonic acid and BPPA-gua (c).

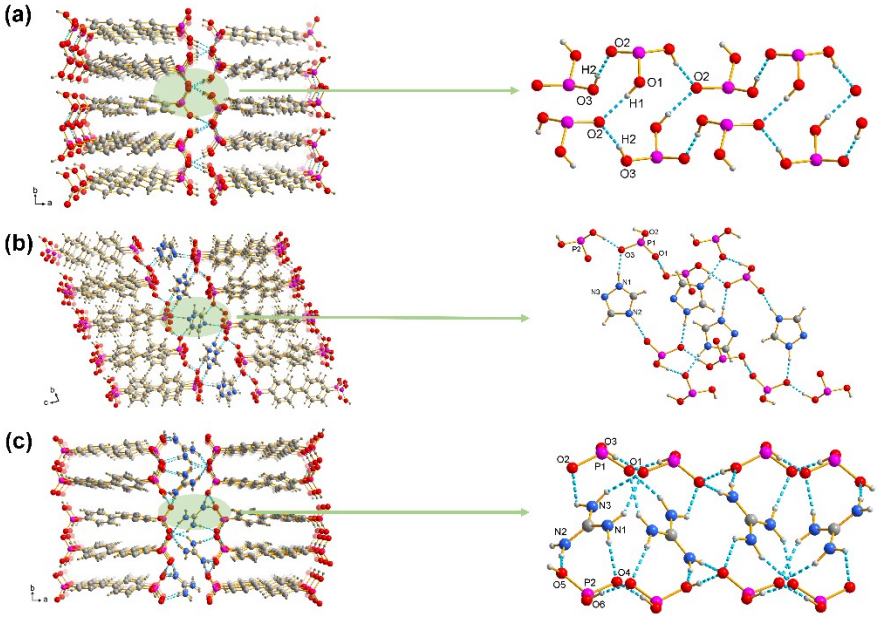

Figure S2. The stacking diagrams and hydrogen bonding networks of (a) BPPA, (b) BPPA-azo and (c) BPPA-gua.

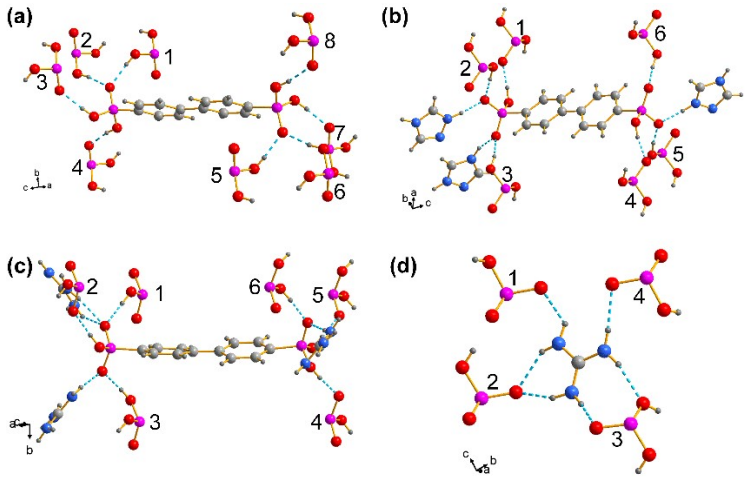

Figure S3. The hydrogen bonds of H_4BPPA molecules in BPPA (a), H_3BPPA^- anions in BPPA-azo (b), H_3BPPA^- anions in BPPA-gua (c), and $HGUA^+$ cations in BPPA-gua (d).

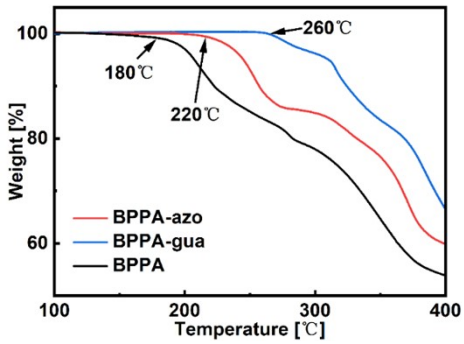

Figure S4. TGA curves of BPPA, BPPA-azo and BPPA-gua.

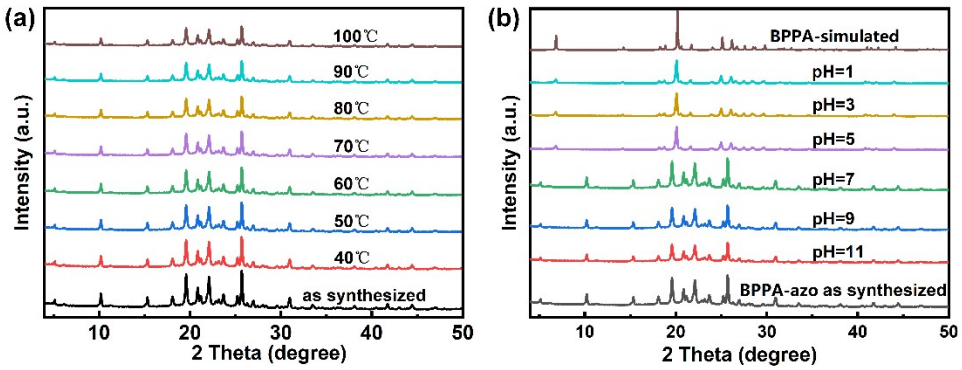

Figure S5. PXRD patterns of BPPA-azo (a) after immersing in solutions of different pH values for 3 d, (b) after immersing in aqueous solutions at different temperatures for 3 d.

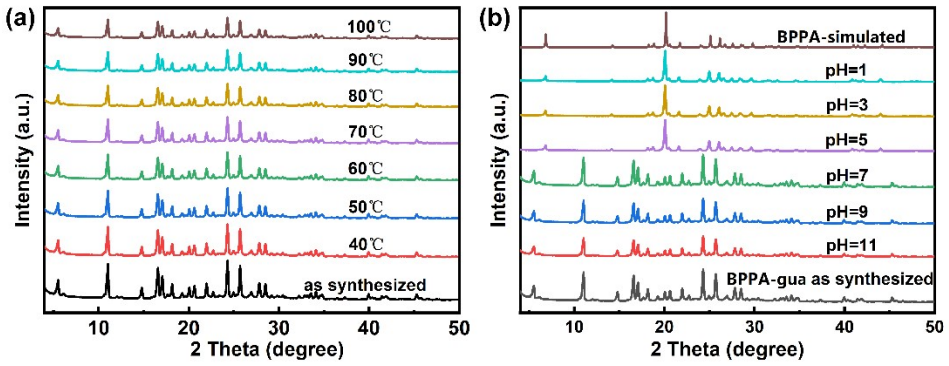

Figure S6. PXRD patterns of BPPA-gua (a) after immersing in solutions of different pH values for 3 d, (b) after immersing in aqueous solutions at different temperatures for 3 d.

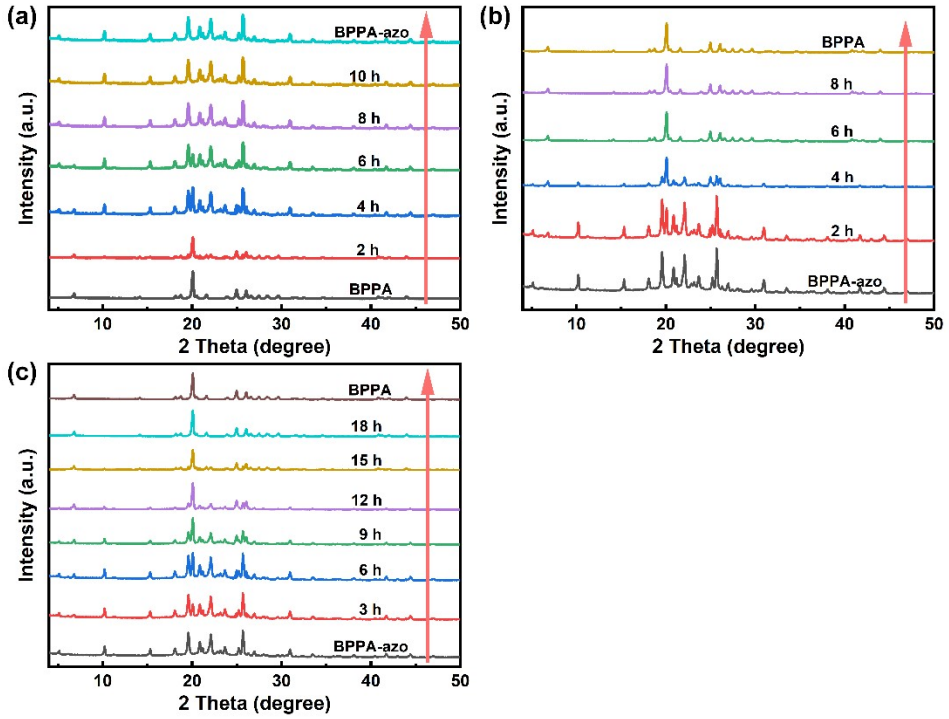

Figure S7. PXRD patterns showing the SCSC transformation time (a) from BPPA to BPPA-azo, (b) from BPPA-azo to BPPA at 100 °C; (c) from BPPA-azo to BPPA at room temperature.

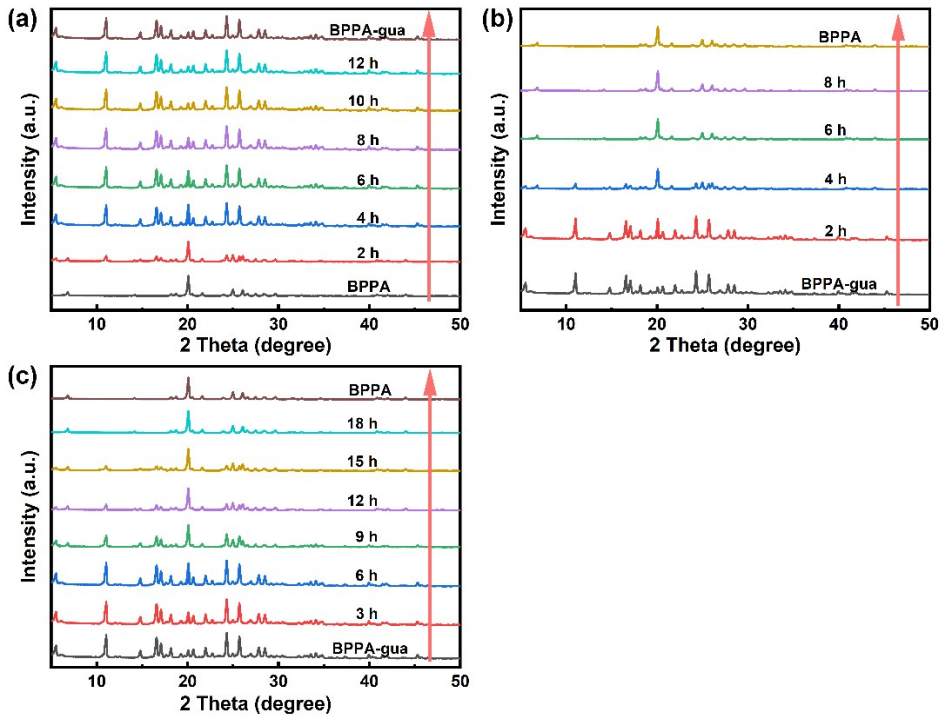

Figure S8. PXRD patterns showing the SCSC transformation time (a) from BPPA to BPPA-gua, (b) from BPPA-gua to BPPA at 100 °C; (c) from BPPA-gua to BPPA at room temperature.

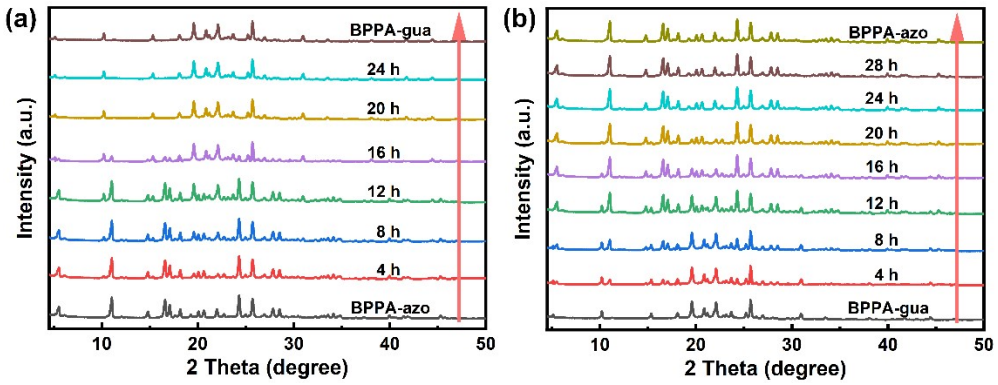

Figure S9. PXRD patterns showing the SCSC transformation time (a) from BPPA-azo to BPPA-gua, (b) from BPPA-gua to BPPA-azo.

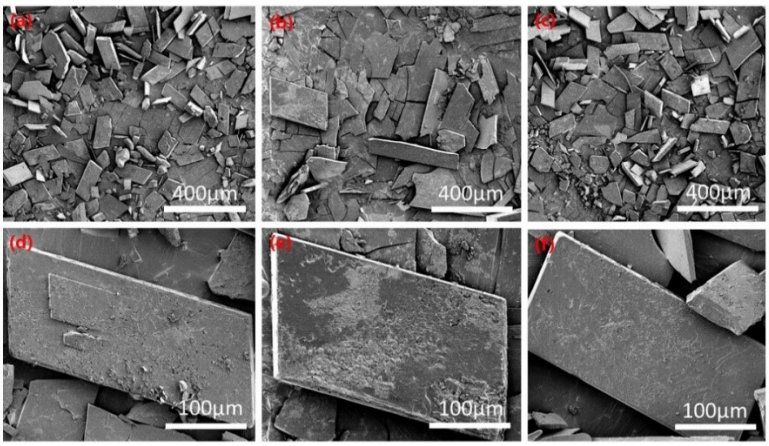

Figure S10. SEM images of (a) BPPA-azo, (b) BPPA-gua and (c) BPPA, Single crystal SEM images of (d) BPPA-azo, (e) BPPA-gua and (f) BPPA.

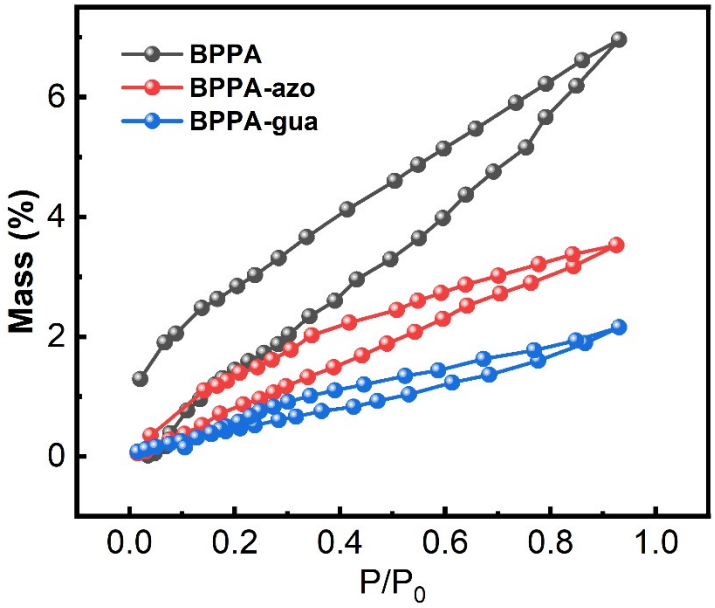

Figure S11. Water sorption isotherms of BPPA, BPPA-azo and BPPA-gua.

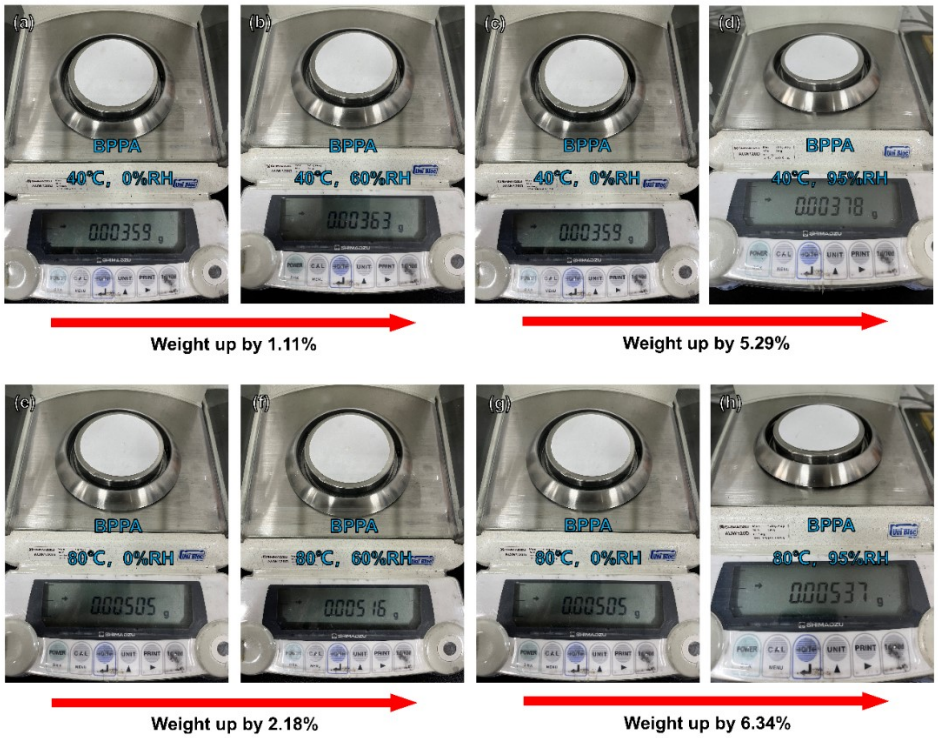

Figure S12. Quality of BPPA pellets at 40 ℃, 0% R.H. (a); at 40 ℃, 60% RH (b); at 40 ℃, 0% RH (c); at 40 ℃, 95% RH (d); at 80 ℃, 0% RH (e); at 80 ℃, 60% RH (f); at 80 ℃, 0% RH (g); at 80 ℃, 95% RH (h). Note: the quality at 0% RH was obtained by weighing immediately after taking the pellet out of the vacuum drying oven, and the quality at other humidity was obtained by weighing immediately after standing the pellets for 2 hours under the related humidity and temperature.

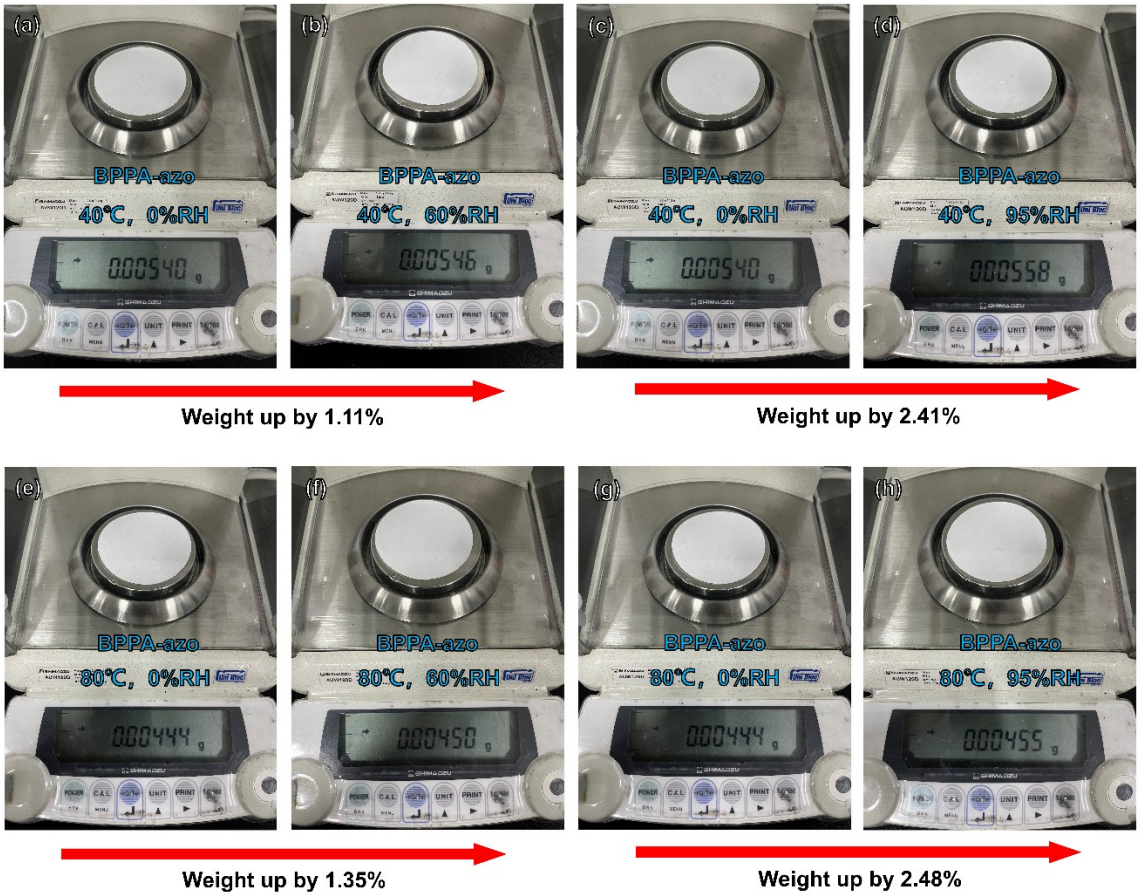

Figure S13. Quality of BPPA-azo pellets at 40 ℃, 0% R.H. (a); at 40 ℃, 60% RH (b); at 40 ℃, 0% RH (c); at 40 ℃, 95% RH (d); at 80 ℃, 0% RH (e); at 80 ℃, 60% RH (f); at 80 ℃, 0% RH (g); at 80 ℃, 95% RH (h). Note: the quality at 0% RH was obtained by weighing immediately after taking the pellet out of the vacuum drying oven, and the quality at other humidity was obtained by weighing immediately after standing the pellets for 2 hours under the related humidity and temperature.

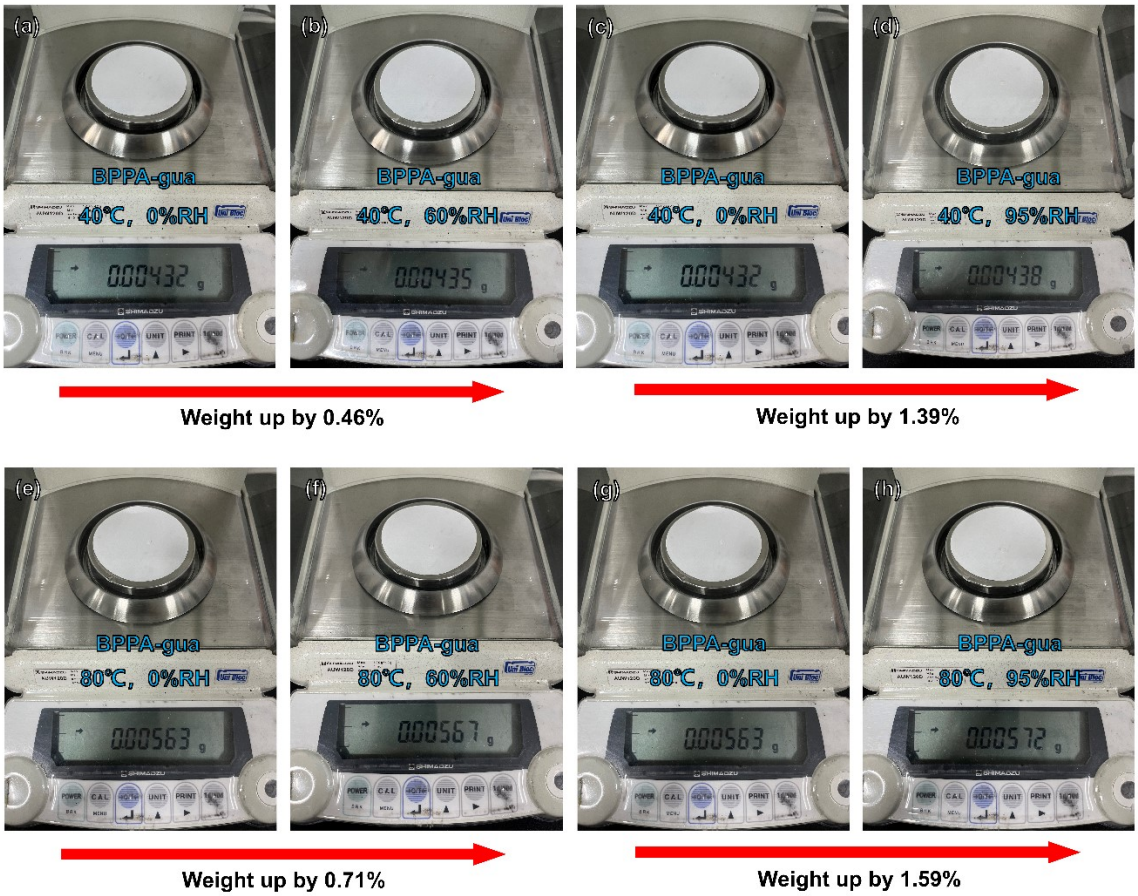

Figure S14. Quality of BPPA-gua pellets at 40 ℃, 0% R.H. (a); at 40 ℃, 60% RH (b); at 40 ℃, 0% RH (c); at 40 ℃, 95% RH (d); at 80 ℃, 0% RH (e); at 80 ℃, 60% RH (f); at 80 ℃, 0% RH (g); at 80 ℃, 95% RH (h). Note: the quality at 0% RH was obtained by weighing immediately after taking the pellet out of the vacuum drying oven, and the quality at other humidity was obtained by weighing immediately after standing the pellets for 2 hours under the related humidity and temperature.

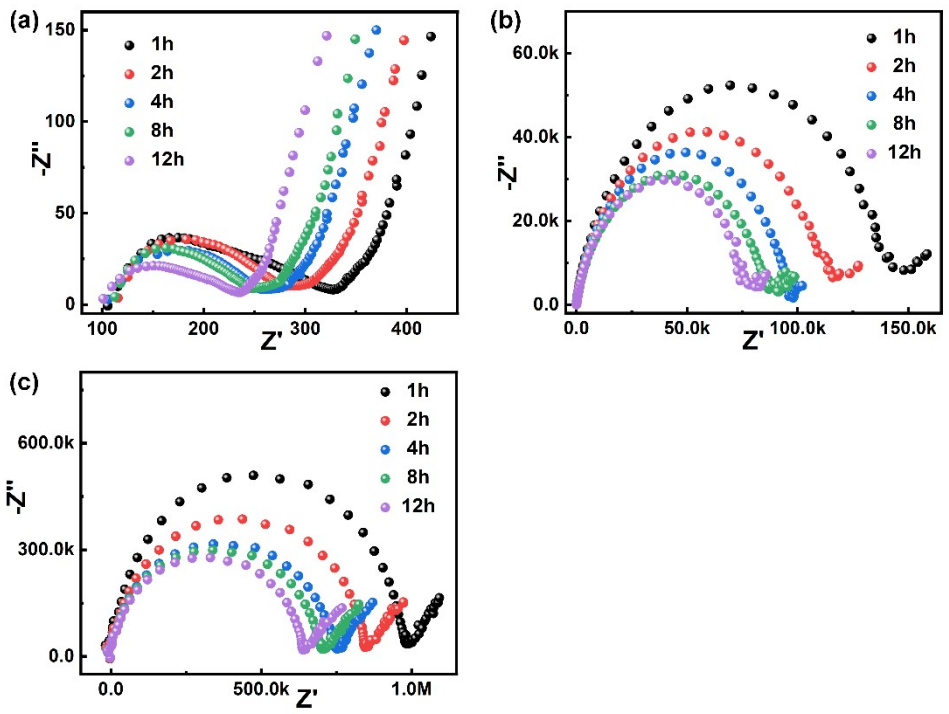

Figure S15. The time-dependent Nyquist plots of (a) BPPA, (b) BPPA-azo, (c) BPPA-gua at 80 °C and 95% RH.

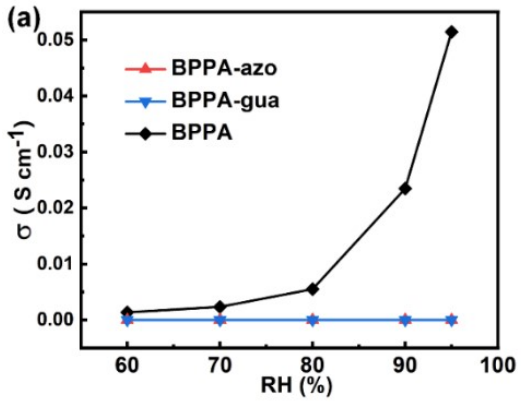

Figure S16. Proton conductivities of BPPA, BPPA-azo and BPPA-gua at 80 °C under different RH.

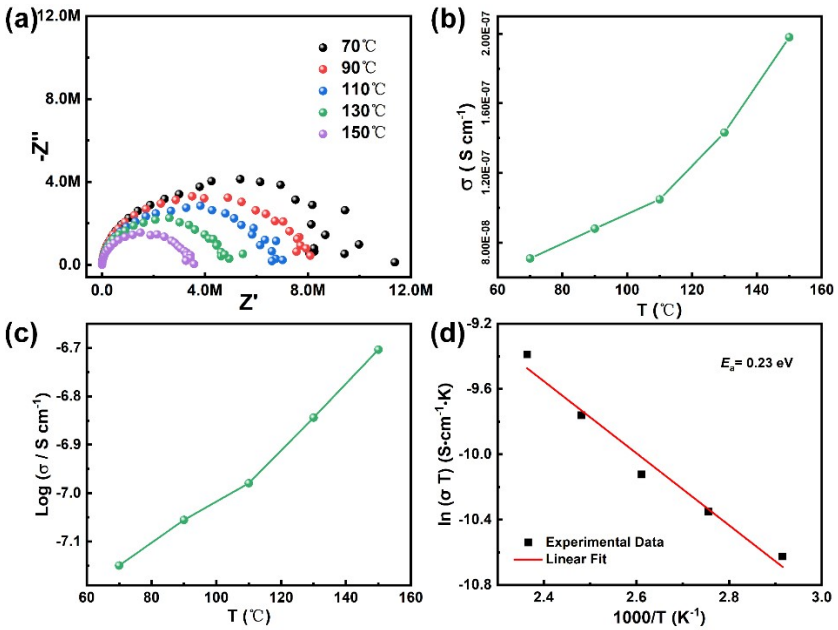

Figure S17. (a) Nyquist plots, (b) Proton conductivities, (c) Log-scaled proton conductivities, and (d) Arrhenius plots of BPPA at various temperatures under anhydrous conditions.

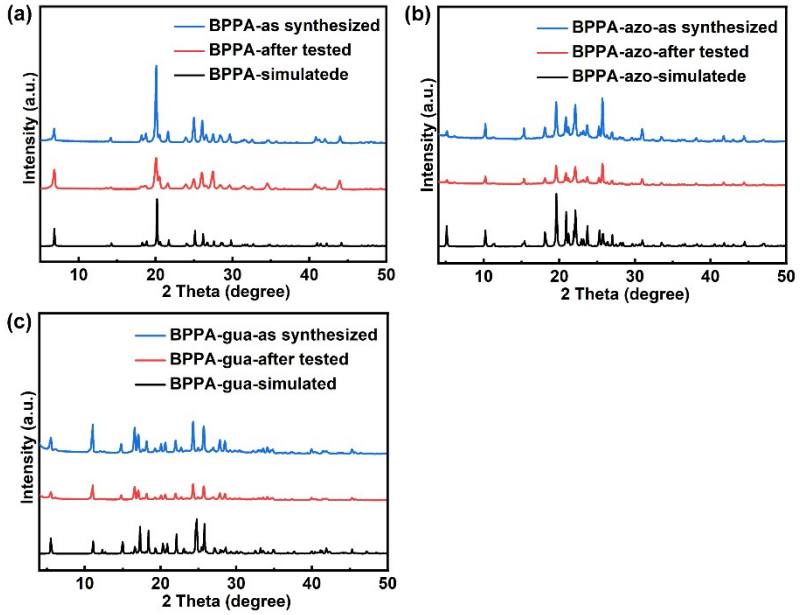

Figure S18. PXRD patterns of (a) BPPA (b) BPPA-azo and (c) BPPA-gua after multiple cyclic humidity-dependent impedance tests at 80 °C and 95% RH.

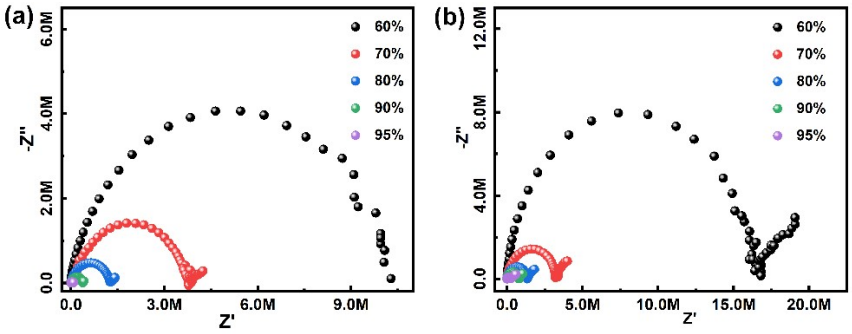

Figure S19. Nyquist plots of (a) BPPA-azo and (b) BPPA-gua under 95% RH at different temperatures.

References

[1] G. ProÂchniak, J. ZonÂ, M. Daszkiewicz, A. Pietraszkob and V. Videnova-AdrabinÂska, Hydrogen-bonded network in biphenyl-4,40-diphosphonic acid, *Acta Cryst.* **2007**, *63*, 434-436.

[2] Y. Qin, T. L. Gao, W. P. Xie, Z. Li and G. Li, Ultrahigh Proton Conduction in Two Highly Stable Ferrocenyl Carboxylate Frameworks, *ACS Appl Mater Interfaces* **2019**, *11*, 31018-31027.

[3] Q. Yang, Y. Wang, Y. Shang, J. Du, J. Yin, D. Liu, Z. Kang, R. Wang, D. Sun and J. Jiang, Three Hydrogen-Bonded Organic Frameworks with Water-Induced Single-Crystal-to-Single-Crystal Transformation and High Proton Conductivity, *Cryst. Growth Des*. **202**0, *20*, 3456-3465.

[4] Z. Yang, Y. Zhang, W. Wu, Z. Zhou, H. Gao, J. Wang and Z. Jiang, Hydrogen-bonded organic framework membrane with efficient proton conduction, *Journal of Membrane Science* **2022**, *664*, 121118.

[5] K. C. Ranjeesh, R. Illathvalappil, S. D. Veer, J. Peter, V. C. Wakchaure, Goudappagouda, K. V. Raj, S. Kurungot and S. S. Babu, Imidazole-Linked Crystalline Two-Dimensional Polymer with Ultrahigh Proton-Conductivity, *J. Am. Chem. Soc.* **2019**, *141*, 14950-14954.

[6] A. Karmakar, R. Illathvalappil, B. Anothumakkool, A. Sen, P. Samanta, A. Desai, S. Kurungot and S. Ghosh, Hydrogen-Bonded Organic Frameworks (HOFs): A New Class of Porous Crystalline Proton-Conducting Materials, *Angew. Chem. Int. Ed.* **2016**, *55*, 10667-10671.

[7] G. Xing, T. Yan, S. Das, T. Ben and S. Qiu, Synthesis of Crystalline Porous Organic Salts with High Proton Conductivity, *Angew. Chem. Int. Ed.* **2018**, *57*, 5345-5349.

[8] M. Yoon, K. Suh, H. Kim, Y. Kim, N. Selvapalam and K. Kim, High and Highly Anisotropic Proton Conductivity in Organic Molecular Porous Materials, *Angew. Chem. Int. Ed.* **2011**, *50*, 7870-7873.

[9] M. Liu, L. Chen, S. Lewis, S. Y. Chong, M. A. Little, T. Hasell, I. M. Aldous, C. M. Brown, M. W. Smith, C. A. Morrison, L. J. Hardwick and A. I. Cooper, Three-dimensional protonic conductivity in porous organic cage solids, *Nat. Commun.* **2016**, *7*, 12750.

[10] L. L. Kang, S. W. Zuo, B. X. Han and G. Li, Comparative study on proton conductivity of a polypyridinyl multicarboxylate-based hydrogen-bonded organic framework and related chitosan composite membrane, *New J. Chem.* **2023**, *47*, 1299-1307.

[11] B. B. Hao, X. X. Wang, C. X. Zhang and Q. Wang, Two Hydrogen-Bonded Organic Frameworks with Imidazole Encapsulation: Synthesis and Proton Conductivity, *Cryst. Growth Des*. **2021**, *21*, 3908-3915.

[12] Z. B. Sun, Y. L. Li, Z. H. Zhang, Z. F. Li, B. Xiao and G. Li, A path to improve proton conductivity: from a 3D hydrogen-bonded organic framework to a 3D copper-organic framework, *New J. Chem.* **2019**, *43*, 10637-10644.

[13] W. Yang, F. Yang, T. L. Hu, S. C. King, H. Wang, H. Wu, W. Zhou, J. R. Li, H. D. Arman and B. Chen, Microporous Diaminotriazine-Decorated Porphyrin-Based Hydrogen-Bonded Organic Framework: Permanent Porosity and Proton Conduction, *Cryst. Growth Des*. **2016**, *16*, 5831-5835.